Mathematical Biosciences 270 (2015) 95–105

Contents lists available at ScienceDirect

Mathematical Biosciences

journal homepage: www.elsevier.com/locate/mbs

Modeling HIV-1 viral capsid nucleation by dynamical systems

Farrah Sadre-Marandi [a,1], Yuewu Liu [b], Jiangguo Liu [a,*], Simon Tavener [a], Xiufen Zou [b]

[a] Department of Mathematics, Colorado State University, Fort Collins, CO 80523-1874, USA
[b] School of Mathematics and Statistics, Wuhan University, Wuhan 430072, Hubei, China

ARTICLE INFO

Article history:
Received 7 May 2015
Revised 8 September 2015
Accepted 9 October 2015
Available online 24 October 2015

Keywords:
Capsid
Dimers
Dynamical systems
Hexamers
HIV-1
Sensitivity analysis

ABSTRACT

There are two stages generally recognized in the viral capsid assembly: nucleation and elongation. This paper focuses on the nucleation stage and develops mathematical models for HIV-1 viral capsid nucleation based on six-species dynamical systems. The Particle Swarm Optimization (PSO) algorithm is used for parameter fitting to estimate the association and dissociation rates from biological experiment data. Numerical simulations of capsid protein (CA) multimer concentrations demonstrate a good agreement with experimental data. Sensitivity and elasticity analysis of CA multimer concentrations with respect to the association and dissociation rates further reveals the importance of CA trimer-of- dimers in the nucleation stage of viral capsid self- assembly.

1. Introduction

Viruses are macromolecular organisms that are composed of infective genetic materials (DNA or RNA) and protective protein shells. Understanding the mechanism in the viral life cycle, particularly the entry, replication, egress, and capsid assembly will be helpful for developing effective treatments of viral diseases. While *in vivo* and *in vitro* approaches offers direct ways for investigating all stages of the viral life cycle, the *in silico* approach (mathematical modeling and computer simulations) plays an increasingly important role in virus studies. Molecular dynamics (MD) is a powerful tool for simulating viral capsid assembly [44] but places high demand on computing resources, although coarse-grain (CG) models, e.g., [10], can reduce the computational cost. In this paper, we explore an inexpensive approach based on the rate equations and dynamical systems.

Dynamical systems or systems of ordinary differential equations have been used for modeling the replication and pathogenesis of human immunodeficiency virus (HIV) [42], HIV virus dynamics [21,31] and infection dynamics of other types viruses [24], including sensitivity analysis of system behaviors to model parameters. But in this paper, we use dynamical systems for modeling the structural biological aspects of HIV. We perform also sensitivity and elasticity analysis for our models. This is a continuation of our efforts in [19,35–37,41] on applying dynamical systems and/or sensitivity analysis as mathematical tools for investigation of biological processes.

HIV-1 is a retrovirus that causes acquired immunodeficiency syndrome (AIDS), a condition in humans in which the immune system fails progressively. It is known that the HIV-1 virion undergoes a maturation process, in which the viral RNA is enclosed by a cone-shape capsid so that the virion becomes infectious. The HIV-1 viral capsid assembly consists of two stages: nucleation and elongation. Understanding the mechanism in the viral capsid assembly is important and will be helpful for developing antiviral therapies that could target viral capsids.

Structural biology research of the HIV-1 virus indicates that HIV-1 conical cores have a lattice structure consisting of hexamers and pentamers [6,9,14,17,34]. At the early stage of viral capsid assembly, lower order CA proteins nucleate into hexamers. These hexamers further assemble into the viral capsid. There have been kinetic models for viral capsid assembly [12,18]. But these models consider a simplified pathway that allows association or dissociation of one capsomer unit at a time. However, there is strong evidence [8,10,16] that dimers associate with other dimers. Moreover, non-monomer subunits can assemble with each other [28,30].

In this paper, we focus on the nucleation stage of viral capsid assembly but consider nearly all possible pathways of association and dissociation. In particular, we develop mathematical models for nucleation using dynamical systems of six species. The biological evidence [7,10,16,25,43] are then used to reduce the model. Published biological experimental data [30] are utilized to estimate the model parameters representing the association and dissociation rates.

* Corresponding author. Tel.: +1 970 491 3067.
E-mail addresses: sadre@math.colostate.edu, sadre.1@mbi.osu.edu (F. Sadre-Marandi), yuewuliu@whu.edu.cn (Y. Liu), liu@math.colostate.edu (J. Liu), tavener@math.colostate.edu (S. Tavener), xfzou@whu.edu.cn (X. Zou).
[1] Current address: Mathematical Biosciences Institute, Ohio State University, Columbus, OH 43210, USA

http://dx.doi.org/10.1016/j.mbs.2015.10.007
0025-5564/

Furthermore, sensitivity and elasticity analysis is performed to find out what association / dissociation terms play more important roles in the nucleation stage.

The rest of this paper is organized as follows. Section 2 presents first a full 6-species model for nucleation kinetics and then a reduced 6-species model. Section 3 discusses the methods for model parameter fitting and sensitivity analysis and elasticity analysis. Section 4 presents results of numerical simulations of CA multimer concentrations along with sensitivity and elasticity analysis. Section 5 concludes the paper with discussion for future work.

2. Models for CA protein nucleation

The existing work in [12,18,26] adopt a straightforward approach by considering one pathway of assembly: only one CA protein (monomer) can assemble with another subunit at a time, that is, from n-mer to $(n+1)$-mer. Similarly, the dissociation is from $(n+1)$-mer to n-mer. However, there is strong evidence [8,10,16] that dimers interact with other dimers. The findings in [28,30] suggest that non-monomer subunits can assemble with each other. Stability analysis in [10] indicates that the dimer is an important CA intermediate in self-assembly.

Based on the aforementioned work, we start with a new model by considering all possible pathways for forming a nucleus, also referred to as a hexamer or 6-mer. We follow the traditional model for polymer growth, which states that any two intermediates can react and join together [33]. Additionally, we add a pathway (b) to mimic the trimer-of-dimers assembly discussed in [7,10,16]. Since dissociation is also important, due to high concentrations of intermediates left after nucleation, more terms are added to describe the multitude of dissociations. We assume that multimers can dissociate in the same way in which they are formed during association.

2.1. A full 6-species model

Listed below are the assumptions for our 6-species model.

1. Nucleation ends with 6-mer formation. Pornilloset al. [28,30] observed little to no existence of c_n, $n > 6$.
2. One forward rate for each intermediate.
3. Multimers can dissociate in the same way they are formed in association.

Based on the above assumptions, a dynamical system of size 6 or a system of six ordinary differential equations is proposed as follows for describing the kinetics in the association and dissociation.

$$\begin{cases} \dfrac{dc_1}{dt} = b_{65}c_6 + b_{54}c_5 + b_{43}c_4 + b_{32}c_3 + 2b_{21}c_2 \\ \qquad - f_{15}c_1c_5 - f_{14}c_1c_4 - f_{13}c_1c_3 - f_{12}c_1c_2 - 2f_{11}c_1^2 \\ \dfrac{dc_2}{dt} = f_{11}c_1^2 + 3b_{62}c_6 + b_{64}c_6 + b_{53}c_5 + 2b_{42}c_4 + b_{32}c_3 \\ \qquad - b_{21}c_2 - 3f_{222}c_2^3 - f_{24}c_2c_4 - f_{23}c_2c_3 - 2f_{22}c_2^2 - f_{12}c_1c_2 \\ \dfrac{dc_3}{dt} = f_{12}c_1c_2 + 2b_{63}c_6 + b_{53}c_5 + b_{43}c_4 - b_{32}c_3 - 2f_{33}c_3^2 \\ \qquad - f_{23}c_2c_3 - f_{13}c_1c_3 \\ \dfrac{dc_4}{dt} = f_{13}c_1c_3 + f_{22}c_2^2 + b_{64}c_6 + b_{54}c_5 - b_{43}c_4 - b_{42}c_4 \\ \qquad - f_{24}c_2c_4 - f_{14}c_1c_4 \\ \dfrac{dc_5}{dt} = f_{14}c_1c_4 + f_{23}c_2c_3 + b_{65}c_6 - b_{54}c_5 - b_{53}c_5 - f_{15}c_1c_5 \\ \dfrac{dc_6}{dt} = f_{15}c_1c_5 + f_{33}c_3^2 + f_{222}c_2^3 + f_{24}c_2c_4 - b_{65}c_6 \\ \qquad - b_{64}c_6 - b_{63}c_6 - b_{62}c_6 \end{cases} \tag{1}$$

where

- c_n is the concentration of the n-mer intermediate ($1 \le n \le 6$);
- f_{ij} is the association rate of c_i and c_j;
- f_{222} is the association rate for trimer-of-dimer;
- b_{ij} is the rate of c_i dissociating into two intermediates with c_j being the larger intermediate of the dissociated terms, b_{62} is for the special case 6-mer dissociates into three dimers.

2.2. A reduced 6-species model

The above full 6-species model considers all possible pathways of two binding intermediates and one triple bond in the association leading to and dissociation down from hexamers. We simplify this model based on the findings in the literature about viral capsid assembly.

1. We consider three main pathways for assembly of a hexamer:
   (a) Single monomers join:
   $$c_1 + c_1 \underset{b_{21}}{\overset{f_{11}}{\rightleftharpoons}} c_2, \quad c_1 + c_2 \underset{b_{32}}{\overset{f_{12}}{\rightleftharpoons}} c_3, \quad c_1 + c_3 \underset{b_{43}}{\overset{f_{13}}{\rightleftharpoons}} c_4,$$
   $$c_1 + c_4 \underset{b_{54}}{\overset{f_{14}}{\rightleftharpoons}} c_5, \quad c_1 + c_5 \underset{b_{65}}{\overset{f_{15}}{\rightleftharpoons}} c_6.$$
   (b) Trimer-of-dimers as illustrated in Fig. 1:
   $$c_1 + c_1 \underset{b_{21}}{\overset{f_{11}}{\rightleftharpoons}} c_2, \quad c_2 + c_2 + c_2 \underset{b_{62}}{\overset{f_{222}}{\rightleftharpoons}} c_6.$$
   (c) Single binding dimers:
   $$c_1 + c_1 \underset{b_{21}}{\overset{f_{11}}{\rightleftharpoons}} c_2, \quad c_2 + c_2 \underset{b_{42}}{\overset{f_{22}}{\rightleftharpoons}} c_4, \quad c_2 + c_4 \underset{b_{64}}{\overset{f_{24}}{\rightleftharpoons}} c_6.$$
2. We consider two pathways for formation of a pentamer:
   (d) Single monomers join (viewed as a part of pathway (a) for hexamers:
   $$c_1 + c_1 \underset{b_{21}}{\overset{f_{11}}{\rightleftharpoons}} c_2, \quad c_1 + c_2 \underset{b_{32}}{\overset{f_{12}}{\rightleftharpoons}} c_3, \quad c_1 + c_3 \underset{b_{43}}{\overset{f_{13}}{\rightleftharpoons}} c_4, \quad c_1 + c_4 \underset{b_{54}}{\overset{f_{14}}{\rightleftharpoons}} c_5.$$
   (e) Dimers and monomers:
   $$c_1 + c_1 \underset{b_{21}}{\overset{f_{11}}{\rightleftharpoons}} c_2, \quad c_2 + c_2 \underset{b_{42}}{\overset{f_{22}}{\rightleftharpoons}} c_4, \quad c_1 + c_4 \underset{b_{54}}{\overset{f_{14}}{\rightleftharpoons}} c_5.$$

It is important to note that the two pathways for formation of a pentamer (d) and (e) do not add new forward or backward rates to the model. Pathway (d) is a subset of pathway (a) for a hexamer, and pathway (e) is a combination of the intermediate pathways found in (a) and (b).

The **hexamer pathways** are based on the findings presented in [25]. The first pathway (a) (monomers join one at a time) was adopted in [12,18,26]. "The symmetric appearance (of a hexamer) is suggestive of symmetric head-to-head dimers" promoting the trimer-of-dimer assembly seen in the second pathway (b), see Fig. 1. This is also advocated in [7,10,16]. The third pathway (c) for a hexamer considered in our reduced model is established based on the discussion in [4,8,15,22,23,25,40]. In particular, [40] asserts that CA prefers to form both dimers and tetramers. This pathway could also be considered as the "slow" formation of trimer-of-dimers. Considering only these three pathways eliminates the parameter f_{33} and the corresponding backward rate b_{63} from the model.

The **pentamer pathways** are also listed, since pentamers are required for formation of a closed viral capsid [3,5,13,27]. Both pathways for pentamer formation occur as either a subpathway or union of hexamer pathways. Note that considering only these two pathways for pentamers allows the elimination of the term $f_{23}c_2c_3$, and its corresponding dissociation term $b_{53}c_5$ from the full model.

Consideration of these pathways reduces emphasis on trimers. Even though trimers of matrix proteins (MA) are predominately observed during the assembly of immature virions [4,41], there is not much evidence that the CA proteins prefer trimer formation [1].

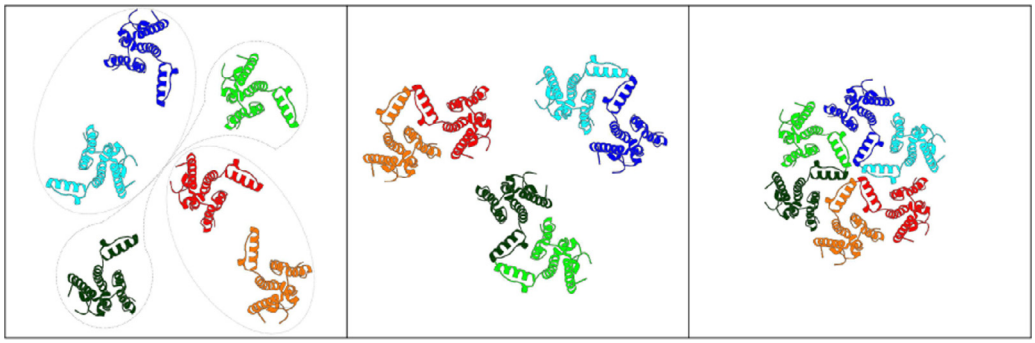

Fig. 1. A diagram for the second pathway (trimer-of-dimers) of hexamer assembly. Protein illustrations are drawn according to the info about PDB 3H47 HIV-1 CA monomer shown in [29] and used by Pornillos et al. [30].

The above discussion leads to **a reduced 6-species model**:

$$\begin{cases} \dfrac{dc_1}{dt} = b_{65}c_6 + b_{54}c_5 + b_{43}c_4 + b_{32}c_3 + 2b_{21}c_2 \\ \qquad - f_{15}c_1c_5 - f_{14}c_1c_4 - f_{13}c_1c_3 - f_{12}c_1c_2 - 2f_{11}c_1^2 \\ \dfrac{dc_2}{dt} = f_{11}c_1^2 + 3b_{62}c_6 + b_{64}c_6 + 2b_{42}c_4 + b_{32}c_3 \\ \qquad - b_{21}c_2 - 3f_{222}c_2^3 - f_{24}c_2c_4 - 2f_{22}c_2^2 - f_{12}c_1c_2 \\ \dfrac{dc_3}{dt} = f_{12}c_1c_2 + b_{43}c_4 - b_{32}c_3 - f_{13}c_1c_3 \\ \dfrac{dc_4}{dt} = f_{13}c_1c_3 + f_{22}c_2^2 + b_{64}c_6 + b_{54}c_5 - b_{43}c_4 - b_{42}c_4 \\ \qquad - f_{24}c_2c_4 - f_{14}c_1c_4 \\ \dfrac{dc_5}{dt} = f_{14}c_1c_4 + b_{65}c_6 - b_{54}c_5 - f_{15}c_1c_5 \\ \dfrac{dc_6}{dt} = f_{15}c_1c_5 + f_{222}c_2^3 + f_{24}c_2c_4 - b_{65}c_6 - b_{64}c_6 - b_{62}c_6 \end{cases} \tag{2}$$

where c_n, f_{ij}, and b_{ij} bear the same meaning as described in the full 6-species model.

This reduced 6-species model will be used for numerical simulations of CA protein nucleation. Sensitivity and elasticity of the intermediate concentrations $c_n (n = 1, \ldots, 6)$ to the forward and backward rates will be analyzed also (see the Section 4).

3. Materials and methods

3.1. An optimization algorithm for model parameter fitting

To obtain values of the model parameters based on published experimental data, we adopt the Particle Swarm Optimization (PSO) method [11]. PSO is a method for optimizing continuous nonlinear functions. PSO has an open-source Matlab implementation, which will be used in this paper to optimize the values of the 16 parameters in the reduced model for viral capsid nucleation under certain constraints on the forward and backward rates.

PSO is a numerical method based on the stochastic optimization technique developed by Eberhart and Kennedy [11] in 1995. Since then, it has been widely used in many research fields, for example, neural network, telecommunications, design, control, signal processing, power systems, and data mining.

PSO optimizes a problem by having a population of candidate solutions (particles). It tries iteratively to improve the solutions with regard to additional constraints by updating generations until the target is met. In each iteration, the solutions are updated by tracking two values: one is the best solution or fitness ($\mathbf{p}$) each parameter has achieved, the other is the best value obtained by any other particle in the population ($g\mathbf{1}$).

After finding the two best values up to that time, the solutions update their velocities and positions by the following formulas:

$$\mathbf{v}(i+1) = w\mathbf{v}(i) + d_1r_1[\mathbf{p}(i) - \mathbf{x}(i)] + d_2r_2[g\mathbf{1}(i) - \mathbf{x}(i)], \tag{3}$$

$$\mathbf{x}(i+1) = \mathbf{x}(i) + \mathbf{v}(i+1), \tag{4}$$

where

- w is the initial inertia weight with a default value 0.9;
- $\mathbf{v}(i)$ is the particle velocity at iteration i;
- d_1, d_2 are the local best influence and global best influence weights, respectively, typically set to $d_1 = d_2 = 2$;
- r_1, r_2 are random variables between (0, 1);
- $\mathbf{x}(i)$ is the particle position at iteration i;
- $\mathbf{p}$, $g\mathbf{1}$ are defined as stated before.

A pseudo code for the procedure is shown as follows.

```
Begin i := 0;
For each particle
Initialize the particle P(i) = {x1, x2, ..., xN};
Calculate the fitness value of P(i);
If fitness value (p) is better than p in history, replace p;
End
Choose the particle with the best fitness value and set as g;
For each particle
Calculate the new velocities and positions (Eqs 3 and 4);
i := i + 1;
End
```

3.2. Constraints on the forward and backward rates

Before using the PSO algorithm to optimize the parameters, an initial guess $P(1)$ must be chosen. The choice of PSO parameters can have a big impact on optimization performance. The following size order relations on the forward and backward rates help find a good initial guess and set bounds for each parameter.

3.2.1. Constraints on the forward rates

The models presented in [12,20,45] assume that only one protein is added (could associate) at a time and all forward rates are equivalent. In [26], it is assumed f_n (equivalent to f_{1n} in our model) increases monotonically with n. In [28], it is found that monomers assemble spontaneously into a hexamer lattice tube, indicating that the CA proteins tend to form hexamers. Based on these studies, we assume that *the forward rates f_{1n} increases with n*.

It is expected that f_{11} *is very small*, since the subunit–subunit interactions are inherently weak [20,43]. The pentamer subunit is the least stable intermediate, so f_{15} *will be relatively large* compared to the others [43].

We adopt a similar size order relation as seen in [26]:

$$f_{11} \leq f_{12} \ll f_{15}. \tag{5}$$

Yeager[43] discusses the stability of intermediates and claims that a hexamer is more stable than a tetramer and a tetramer is more stable than a pentamer. We assume that stability helps drive intermediate formation and accordingly

$$f_{22} \leq f_{24} \ll f_{15}. \tag{6}$$

For the reduced nucleation model presented in this paper, all the forward rates except f_{222} have the physical dimension $T^{-1}L^3M^{-1}$, where T is time, L is length, and M is mass. The forward rate f_{222} (for trimer-of-dimer) is the only rate that has a physical dimension $T^{-1}(L^3M^{-1})^2$. It cannot be simply compared to the other forward rates. Chen andTycko [10] note that the trimer-of-dimers structure is crucial for lattice formation, and [8,16] found hexameter formation occurs with increased CA dimer concentration, so *it is expected f_{222} to be large*.

3.2.2. Constraints on backward rates

All the backward rates have the physical dimension T^{-1}.

The discussion in [8,10,16] implies that it is less likely for a dimer to dissociate. Hence, we assume that b_{21} will be the smallest backward rate. Additionally, the instability of pentamers [43] implies that b_{65} should be low compared to that of other hexamer dissociations. These lead to the following assumptions

$$b_{21} \leq b_{65} \leq b_{64}, \tag{7}$$

$$b_{21} \leq b_{65} \leq b_{62}. \tag{8}$$

3.3. Sensitivity and elasticity analysis

Sensitivity analysis examines how a system responds to the changes in its parameters. Sensitivity analysis is useful for identifying important parameters that require additional investigation or insignificant parameters that could be eliminated from a model [37,41].

Sensitivity is computed by finding the derivatives of each variable with respect to each parameter. In other words, the sensitivity of the ith variable (c_i) with respect to the kth parameter (p_k) is defined as

$$S_{i,k} = \frac{\partial c_i}{\partial p_k}, \quad i = 1, \ldots, N, \; k = 1, \ldots, K, \tag{9}$$

where N is the size of the system and K is the dimension of the parameter space.

Writing a dynamical system as a parametric ODE system

$$\frac{dc_i}{dt} = h_i(\mathbf{c}, \mathbf{p}), \quad i = 1, \ldots, N; \; \mathbf{p} \in \mathbb{R}^K, \tag{10}$$

we have the sensitivity of all variables (c_i) with respect to all parameters when the following ODE system is solved:

$$\frac{dS_{i,k}}{dt}(t) = \left(\sum_{n=1}^{N} \frac{\partial h_i}{\partial c_n} S_{n,k}(t) \right) + \frac{\partial h_i}{\partial p_k}(t), \qquad S_{i,k}(0) = 0. \tag{11}$$

However, sensitivity analysis may yield misleading results when the parameter values change greatly in magnitude. Elasticity can produces more reliable results. Elasticity describes the rate of change of the relative size of the variable with respect to the relative size of the parameter. The elasticity of the ith variable with respect to the kth parameter is defined as

$$E_{i,k}(t) = \frac{p_k}{c_i(t)} \frac{\partial c_i}{\partial p_k}(t). \tag{12}$$

SENSAI [38] is a freely available MATLAB package for performing a forward sensitivity and/or elasticity analysis on parameterized systems of nonlinear dynamical systems. SENSAI evaluates the Jacobian

$$\frac{\partial h_i}{\partial c_n}, \quad i, n = 1, \ldots, N \tag{13}$$

and the partial derivatives with respect to the parameters

$$\frac{\partial h_i}{\partial p_k}, \quad i = 1, \ldots, N, \; k = 1, \ldots, K \tag{14}$$

symbolically using MuPAD, then solves Eq. (11) in MATLAB.

4. Results

We first describe the data used for comparison for the model presented in this paper. Parameter fitting is performed for the reduced 6-species model with the parameter constraints explained in Section 3.2 so that the solution of the dynamical system closely matches the experimental data reported in [30]. Numerical simulations are performed. Then sensitivity and elasticity of n-mer concentrations to parameters are examined.

4.1. Use of biological experimental data

It is known from the discussion in [28,30,43] that the structures of CA hexamers are very difficult to obtain because of the weak interactions holding the hexamers together. Instead mutant CA hexamers were utilized for experiments.

Pornillos et al. [28] compare each mutant hexamer to the HIV-1 CA hexamer given by the Protein Data Bank (PDB) code 3dik. It is found that four mutants assembling into tubes “appeared similar in morphology to the wild-type tubes”. Of the four, only two mutants (A14C/E45C in lane 3 and A42C/T54C in lane 9) have enriched 6-mer bands, which is favorable for hexamer bonding to create the full lattice.

Pornillos et al. [28] state that A14C/E45C produces hexamers that are the most similar to wild-type HIV-1 hexamers, and adding two more mutations gives the construct A14C/E45C/W184A/M185A even more favorable results. However, no data is reported for this construct.

Pornillos et al. [30] present a similar study, creating mutant CA protein that faithfully mimic the hexamer properties of HIV-1 capsid. It is found that the same two mutants A14/E45 and A14C/E45C/W184A/M185A produce the most realistic results. In this case, it is found that the latter mutant assemble less efficiently than A14C/E45C alone.

Both [28,30] consider hexamers stabilized by engineering disulfide cross-link (the mutation) A14/E45 with similar results. Pornillos et al. [30] give more information about the protein concentration and timing.

In [30], crosslinked CA A14C/E45C hexamers were prepared by 10 mg/mL protein into assembly buffer. The buffer is given sequentially, first with 200 mM β-mercaptoethanol (βME), then 0.2 mM βME, and lastly 20 mM Tris (pH 8). Each step is performed for 8 h.

For this paper, we use the data shown in Fig. 1 Panel D line 5 in [30] (reprinted in this paper as Fig. 2 the right panel). In particular, we utilize the image processing software ImageJ to process the information in the aforementioned image. Each i-mer was measured five times to alleviate any discrepancies due to any error occurring in the measuring process. The average of these measurements are used as our ideal equilibrium concentrations.

4.2. Results of model parameter fitting

The initial guess and bounds are constructed using the relationships defined in Section 3.2. PSO is run 10 times due to the randomness involved in Eq. (3). Weights are set to the conventional values, with $d_1 = d_2 = 2$ and $w = 0.9$. Iterations are terminated after the max number of iterations ($i = 2000$) or by hitting the minimum global error

$$|g(i+1) - g(i)| < 1 \times 10^{-25} \tag{15}$$

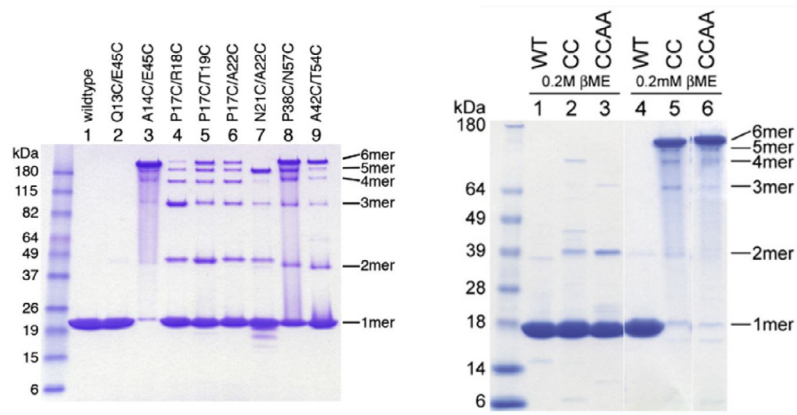

Fig. 2. Experimental data of intermediate concentrations. (Left) SDS-PAGE profiles of the assembly. Source: [28] (reprinted with permission from Elsevier). (Right) WT stands for wild type, CC corresponds to A14C/E45C, and CCAA is A14C/E45C/W184A/M185A. Source: [30] (reprinted with permission from Elsevier).

Table 1
Optimal model parameter values used for numerical simulations.

$f_{11} = 0.000556$	$f_{12} = 0.004506$	$f_{13} = 0.000867$	$f_{14} = 0.038226$
$f_{15} = 0.179675$	$f_{22} = 0.013196$	$f_{222} = 0.159765$	$f_{24} = 0.061905$
$b_{65} = 0.193838$	$b_{64} = 0.256905$	$b_{62} = 0.993826$	$b_{54} = 0.056015$
$b_{43} = 0.728455$	$b_{42} = 0.719905$	$b_{32} = 0.717905$	$b_{21} = 0.019094$

Table 2
Real equilibria for Eq. (2) evaluated with parameters defined in Table 1.

$(c_1,$	$c_2,$	$c_3,$	$c_4,$	$c_5)$
(−6.43E+60,	4.02E+59,	4.017E+59,	6.28E+57,	−1.93E+07)
(7.29E+20,	−1.24E+20,	−5.13E+19,	−2.70E+17,	−6.43E+04)
(−5.94E+10,	1.74E+10,	5.97E+09,	8.52E+07,	−1.47E+04)
(−0.419 ,	−8.976 ,	−53.623 ,	−55.321 ,	891.872)
(12.846 ,	6.476 ,	17.524 ,	18.613 ,	10.456)
(−360.795 ,	7.256 ,	57.058 ,	−0.787 ,	−0.483)

with a minimum of 250 successive iterations.

We choose the set of parameters that minimize the error between the experimental data and the numerical solution. The optimized parameters yield the lowest relative error (0.0125) are listed in Table 1. All the forward rates except f_{222} have the physical dimension $T^{-1}L^3M^{-1}$, where T is time, L length, and M mass. The forward rate f_{222} has a physical dimension $T^{-1}(L^3M^{-1})^2$. All backward rates have the physical dimension T^{-1}. For the numerical simulations in this paper, we use the following units: second for time T, millimeter for length L, and milligram for mass M.

4.3. Results of multimer concentrations (c_1, c_2, c_3, c_4, c_5, c_6)

Now we discuss the stability of equilibria for the reduced 6-species model (see Fig. 3). First, we reduce the system according to the mass conservation law and our initial condition is $\vec{c}(0) = (1300, 0, 0, 0, 0, 0)$. This means

$$c_1 + 2c_2 + 3c_3 + 4c_4 + 5c_5 + 6c_6 = 1300. \tag{16}$$

The equilibria of the mass-conserving model are found using the `solve` function in MATLAB. Due to the complexity of the model, the parameters are first set to the optimized parameters (Table 1). Then, each equation in the model is set to zero to be solved for the concentration values. Seventeen solutions were found, out of which six were real-valued, as listed in Table 2. The negative and imaginary equilibrium points are discarded, since they are not biologically meaningful. This reduces the number of biologically possible equilibria to just one (line 5 in Table 2). The Jacobian of the system is then computed and evaluated at this equilibrium. The eigenvalues are found to be as follows:

$$\lambda_1 = -3.196, \lambda_2 = -4.600, \lambda_3 = -179.051, \lambda_4 = -0.886 - 0.342i, \lambda_5 = -0.886 + 0.342i.$$

Since, each eigenvalue has a negative real part, the equilibrium shown in Fig. 4 is stable.

The monomer concentration c_1 quickly decreases as the CA proteins bind with c_i concentrations to form c_{i+1} intermediates. Note that there is a large initial spike in the dimer concentration c_2, implying many monomers bind together to form dimers first, as discussed in [4,8,15]. The quick decrease in c_2 indicates the importance of the dimers in building higher order n-mers. It is interesting to see the trimer concentration c_3 goes through an initial spike then a drop and then approaches the equilibrium. This will be further addressed in the section on embedded modeling. The concentrations $c_n (n = 4, 5, 6)$ are gradually increasing as expected.

4.4. Results of sensitivity and elasticity analysis

Sensitivity and elasticity analysis is performed for the concentration of n-mer c_n $(n = 1, 2, 3, 4, 5, 6)$ with respect to the association and dissociation rates (forward and backward rates) using the SENSAI Matlab package [38]. There are a total of 16 forward and backward rates, as shown in Fig. 5.

As shown in Table 1, the model parameter values vary in three orders of magnitude. This suggests that a scaling of the parameter values is necessary and elasticity analysis may be more appropriate than just sensitivity analysis.

For the six concentrations $c_i (i = 1, \ldots, 6)$ and the sixteen parameters $p_k (k = 1, \ldots, 16)$, a total of 96 derivatives need to be calculated over time. A scaling is then executed as defined in Eq. (12) to obtain the elasticity.

We examine the elasticity of the concentrations to the model parameters at the following times: $t = 1 \times 10^{-5}, 0.03, 0.1, 1, 2, 4, 7, 12$ (s). We consider the values at $t = 12$ as the equilibrium values. There are rapid changes in the concentration of monomers for $t < 1$ and so we consider elasticity at three other times before $t = 1$, then three other times after $t = 1$ but before the equilibrium.

The elasticity results tell an expected story. Near the beginning (Fig. 5), concentrations are most elastic to the forward rates, especially f_{11}. This is intuitive, since the c_1 concentration is rapidly decreasing as the monomers are forming into dimers and trimers, as demonstrated in the spikes of c_2 and c_3 concentrations in Fig. 4. As the time increases, concentrations become less elastic to these forward rates but more elastic towards those higher intermediate forward rates, such as f_{14} and f_{15} (Fig. 5 row 2).

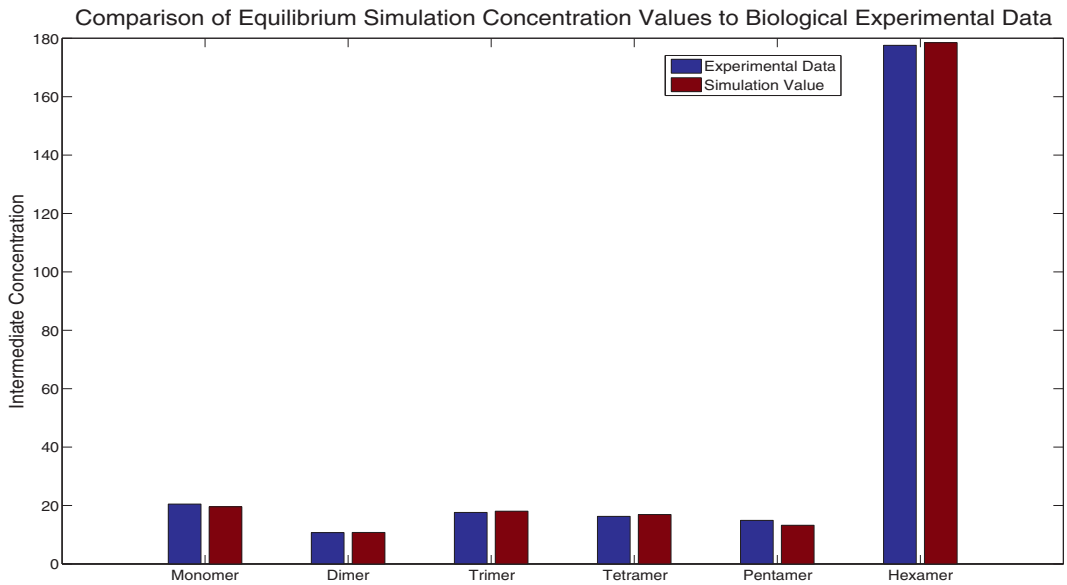

Fig. 3. Concentrations of all intermediates $c_n (1 \le n \le 6)$ at simulation time $t = 24 \times 3600$ (s) with initial values $(c_1(0), c_2(0), c_3(0), c_4(0), c_5(0), c_6(0)) = (1300, 0, 0, 0, 0, 0)$. The simulation results with optimized model parameters (shown in dark red) demonstrate good agreement with the experimental data in [30], 24 h after the experiment (shown in dark blue). (For interpretation of the references to color in this figure legend, the reader is referred to the web version of this article).

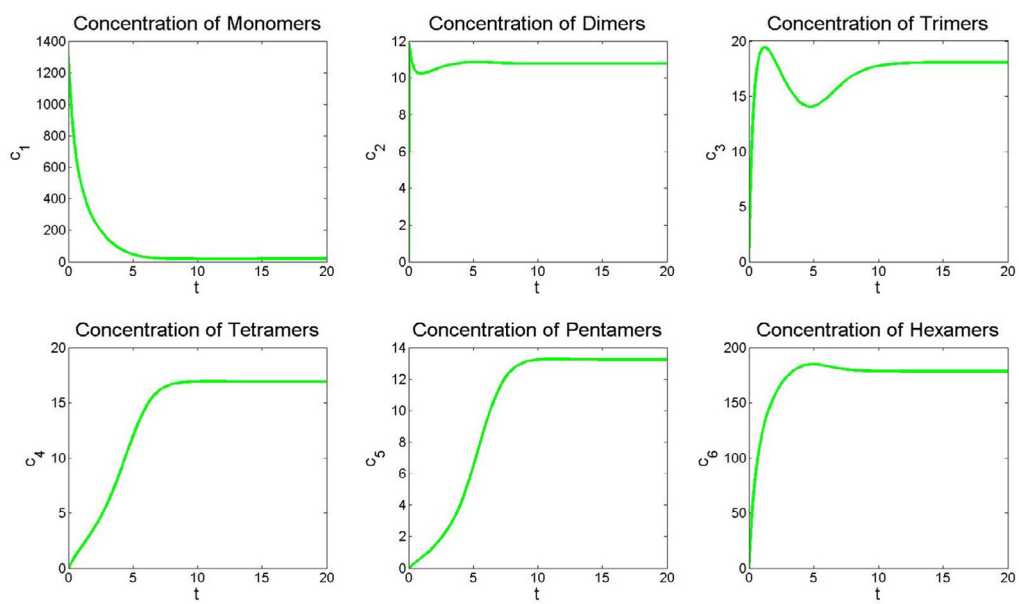

Fig. 4. Simulation results: concentrations of all intermediates $c_n (1 \le n \le 6)$ from simulation time $t = 0$ to $t = 20$ (s) with an initial condition $\vec{c}(0) = (c_1(0), c_2(0), c_3(0), c_4(0), c_5(0), c_6(0)) = (1300, 0, 0, 0, 0, 0)$. Simulations were performed until $t = 24 \times 3600$ (s), though they are not shown here due to the early convergence of the solution.

There is a comparable increase in elasticity to the backward rates (Fig. 5 rows 3 and 4). It is interesting to note that the elasticity to parameters b_{65} and b_{64} appear first out of the backward rates (Fig. 5 row 1 right), and remain evident throughout the rest of the simulation time period. Since hexamers are assumed to be the most stable intermediate, these results could provide information on when hexamers might disassemble.

Elasticity to the association rates f_{1i}, $i = 1, \ldots, 6$. The hexamer concentration c_6 shows the largest elasticity to the forward rate f_{11} at the beginning of nucleation. Other concentrations also show elasticity to f_{11} at times as expected, since f_{11} is the parameter needed for nucleation to begin. These elasticities decrease as time increases, except for concentrations c_1, c_4, for which some fluctuations are observed. See Fig. 5 (rows 1 and 2) for c_1 and Fig. 5 (row 3 right) for c_1, c_4. All other intermediate concentrations follow a similar pattern of decreasing in elasticity for the forward rate f_{12}.

The elasticity of c_5 to f_{14} is seen at the beginning (Fig. 5 row 1 left). It gradually increases as time goes by and the system approaches its equilibrium (Fig. 5 rows 3 and 4). Concentration of c_5 also shows consistent elasticity towards parameter f_{15}. This implies that the two forward rates f_{14}, f_{15} are important for the assembly of a pentamer and hexamer. Minimal elasticity is observed for any concentration with respect to f_{13}.

Elasticity to the association rates f_{22}, f_{222}, f_{24}. Concentrations c_4, c_5 both demonstrate elasticity with respect to parameter f_{22} at the beginning of nucleation (Fig. 5 row 1). These elasticities decrease as time increases. A similar pattern is seen for c_6 with respect to f_{222} as the system approaches its equilibrium. These results can be viewed

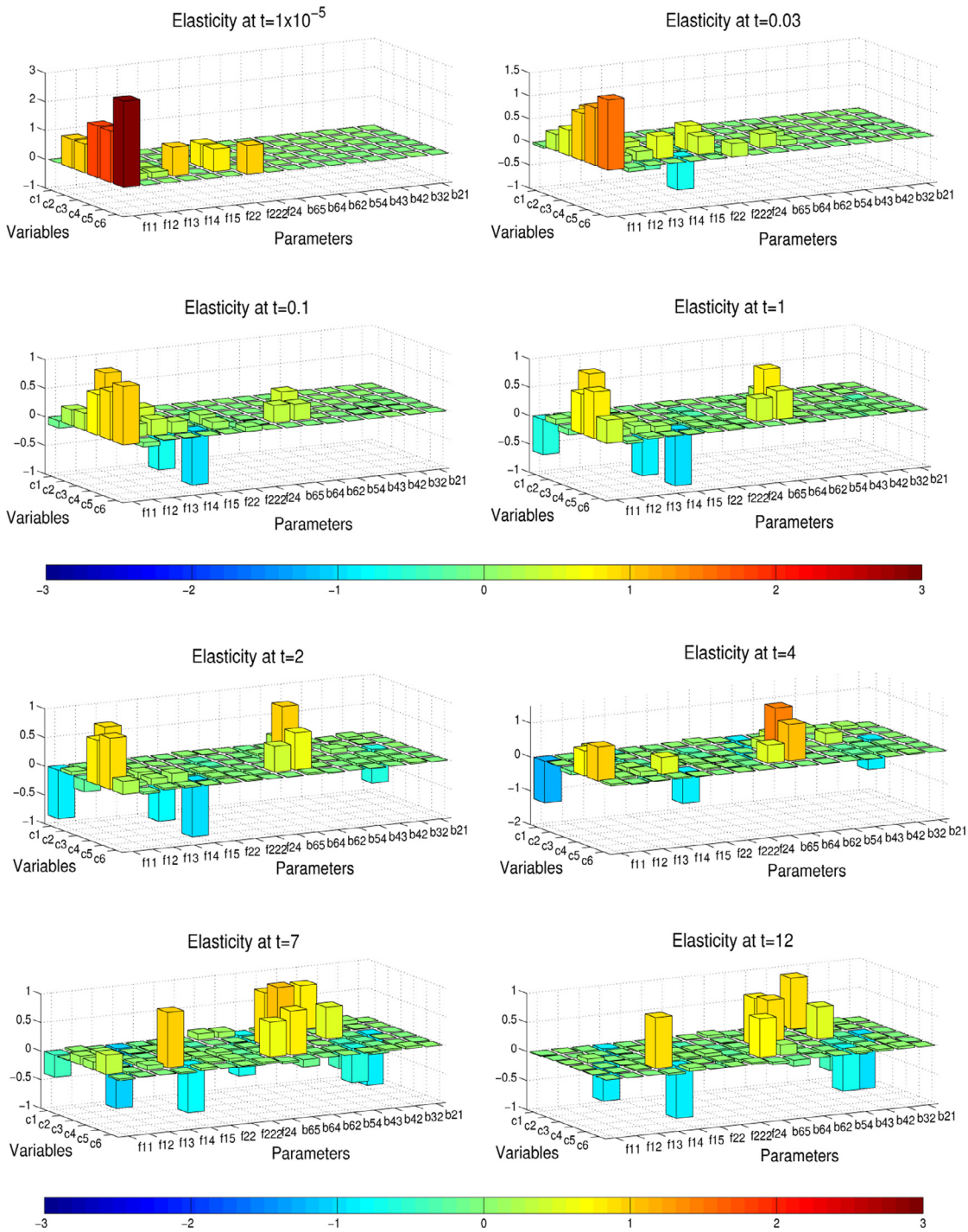

Fig. 5. Elasticities of the n-mer concentration c_n with respect to the association and dissociation rates are plotted for eight simulation time moments: $t = 1 \times 10^{-5}$, 0.03, 0.1, 1, 2, 4, 7, 12 (s).

as indications of the importance of the dimer intermediate in the assembly (pathways (b) and (c)).

Elasticity to the backward rates. As shown in Fig. 5, the magnitude of elasticities with respect to the backward rates tends to increase whereas the magnitude of elasticities with respect to the forward rates decreases. Elasticity to the backward rate b_{65} appears first (see Fig. 5 rows 1 and 2) and stays evident as time increases. Concentration c_3 has consistent elasticity past $t = 2$ and c_4 has consistent elasticity with respect to b_{43} from $t = 7$ to the equilibrium. These results indicate that higher order multimers may prefer disassembly of one monomer at a time.

Concentrations c_4 and c_5 show elasticity to parameter b_{64}. This is expected for c_4, since the backward rate b_{64} is representative of a hexamer dissociating into a tetramer and dimer. The elasticity of c_5 with respect to b_{64} may be indicative of a pentamer being integrated into the lattice, as discussed in [43]. Minimal elasticity is seen for any concentration with respect to parameters b_{62}, b_{54}, b_{42}, b_{21}.

4.5. Model sensitivity and embedded models

Consistent low elasticity over time could imply that certain parameters are not important for modeling capsid nucleation. These

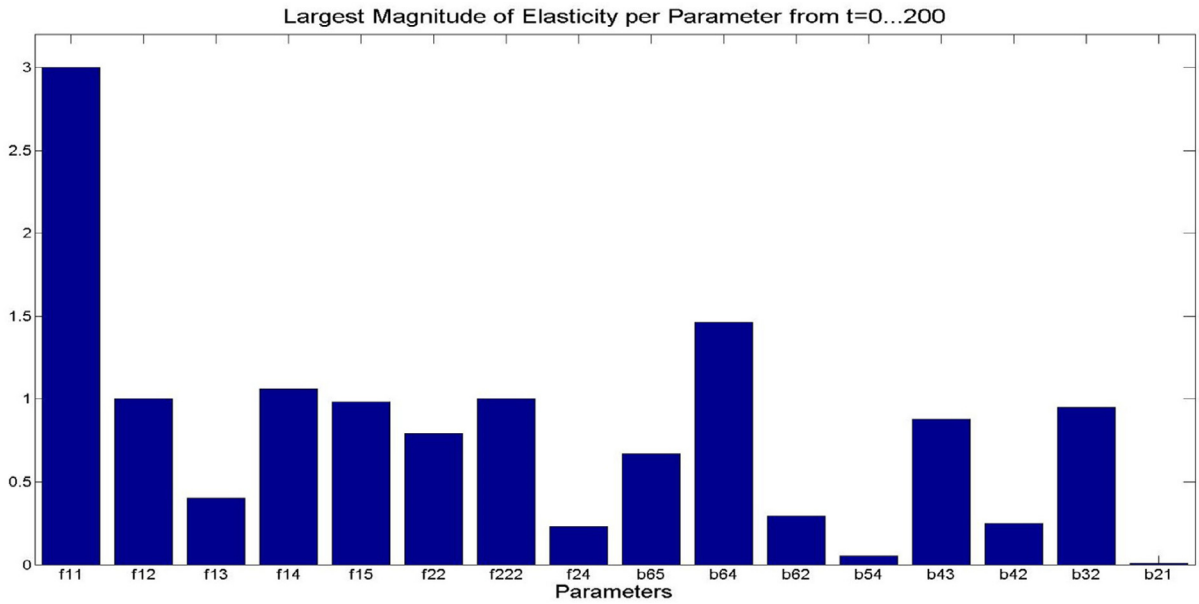

Fig. 6. The largest elasticity magnitudes for the n-mer concentration c_n with respect to the model parameters over all time (represented by the magnitudes of the derivative). Low elasticity is observed for parameters $f_{13}, f_{24}, b_{62}, b_{54}, b_{42}, b_{21}$.

Table 3
Relative error by removing individual parameters.

Parameters	f_{13}	f_{24}	b_{62}	b_{54}	b_{42}	b_{21}
Relative error $\frac{\|\|X_r-X\|\|}{\|\|X\|\|}$	0.0034	0.0479	0.0314	0.0075	0.0537	0.0020

Table 4
Relative error by removing multiple parameters simultaneously.

Parameters	f_{13}, b_{54}	f_{13}, b_{21}	b_{54}, b_{21}	f_{13}, b_{54}, b_{21}
Relative error $\frac{\|\|X_r-X\|\|}{\|\|X\|\|}$	0.0048	0.0021	0.0095	0.0068

parameters may not give additional or important information for our model. To validate this claim, **embedded models** are analyzed to further characterize which parameters are most important for reflecting the assembly kinetics. Parameters with low elasticity are removed from the model, one at a time, to analyze its importance in the model. A parameter is deemed important only if the equilibrium solution changes or the time to equilibrium changes drastically.

The largest magnitude of the elasticity for each concentration c_n with respect to parameter p_k for $0 < t < 200$ is shown in Fig. 6. We identify parameters with low elasticity for all concentrations c_n. The parameters of question are taken to be $f_{13}, f_{24}, b_{62}, b_{54}, b_{42}$ and b_{21}.

Each parameter is removed from the model, one at a time. The dynamical system is then reduced and re-solved. Equilibrium solution is evaluated and the relative error between the new equilibrium (X_r) and the original model equilibrium (X) is calculated. The results from the embedded models are listed in Table 3. It is observed that parameters f_{13}, b_{54}, b_{21} can be eliminated from the model individually with negligible changes to the equilibrium concentrations.

This process is repeated by removing multiple parameters simultaneously. The relative error of removing multiple parameters are listed in Table 4. It is clear that the three parameters f_{13}, b_{54}, b_{21} can be eliminated from the model simultaneously with a negligible change to the equilibrium concentrations. By removing all three parameters, the three main pathways for assembly of a hexamer change. The new pathways are listed below.

(a') Single monomers join (reduced):

$$c_1 + c_1 \xrightarrow{f_{11}} c_2, \quad c_1 + c_2 \underset{b_{32}}{\overset{f_{12}}{\rightleftharpoons}} c_3, \quad c_1 + c_3 \underset{b_{43}}{\leftharpoonup} c_4,$$
$$c_1 + c_4 \xrightarrow{f_{14}} c_5, \quad c_1 + c_5 \underset{b_{65}}{\overset{f_{15}}{\rightleftharpoons}} c_6.$$

(b') Trimer-of-dimers (reduced):

$$c_1 + c_1 \xrightarrow{f_{11}} c_2, \quad c_2 + c_2 + c_2 \underset{b_{62}}{\overset{f_{222}}{\rightleftharpoons}} c_6.$$

(c') Single binding dimers (reduced):

$$c_1 + c_1 \xrightarrow{f_{11}} c_2, \quad c_2 + c_2 \underset{b_{42}}{\overset{f_{22}}{\rightleftharpoons}} c_4, \quad c_2 + c_4 \underset{b_{64}}{\overset{f_{24}}{\rightleftharpoons}} c_6.$$

By removing parameters b_{54}, b_{21}, pentamers and dimers are no longer able to dissociate in the new model. Similarly, by removing parameter f_{13}, there is only one pathway for tetramer assembly (pathway (c'), two dimers forming a tetramer). It is interesting to note that all three of these parameters are found in the traditional pathway (a), as discussed in the studies presented in [18,45]. Removal of these parameters disrupts this pathway.

Calculating the probability of each pathway would be helpful for identifying the usefulness of the traditional pathway in the existing work, compared to the two new pathways for hexamer assembly investigated in this paper: single binding dimers (pathway (c)) and the trimer-of-dimer (pathway (b)).

4.6. Full model vs reduced model

In Section 2.1, we proposed a full model for HIV-1 capsid nucleation by considering theoretically possible pathways. A reduced model is derived in Section 2.2 by eliminating certain pathways based on biological evidence in the literature that these pathways are less likely. In Sections 4.2–4.4, we conducted numerical simulations as well as sensitivity and elasticity analysis to examine which parameters in the reduced model are less significant. Then further reductions of the reduced model were examined to verify that indeed these further reduced models (or embedded models) can still catch the main features of the association and dissociation processes.

Table 5
Comparison of fitted values for the parameters in the full and reduced models.

	Full	Reduced		Full	Reduced		Full	Reduced
f_{11}	0.000498	0.000556	b_{65}	0.205719	0.193838	f_{23}	0.001434	N/A
f_{12}	0.004585	0.004506	b_{64}	0.263029	0.256905	f_{33}	0.001092	N/A
f_{13}	0.000830	0.000867	b_{62}	0.960900	0.993826	b_{63}	0.012523	N/A
f_{14}	0.040147	0.038226	b_{54}	0.109395	0.056015	b_{53}	0.004154	N/A
f_{15}	0.169364	0.179675	b_{43}	0.556444	0.728455			
f_{22}	0.013115	0.013196	b_{42}	0.738419	0.719905			
f_{222}	0.161355	0.159765	b_{32}	0.685344	0.717905			
f_{24}	0.106903	0.061905	b_{21}	0.028071	0.019094			

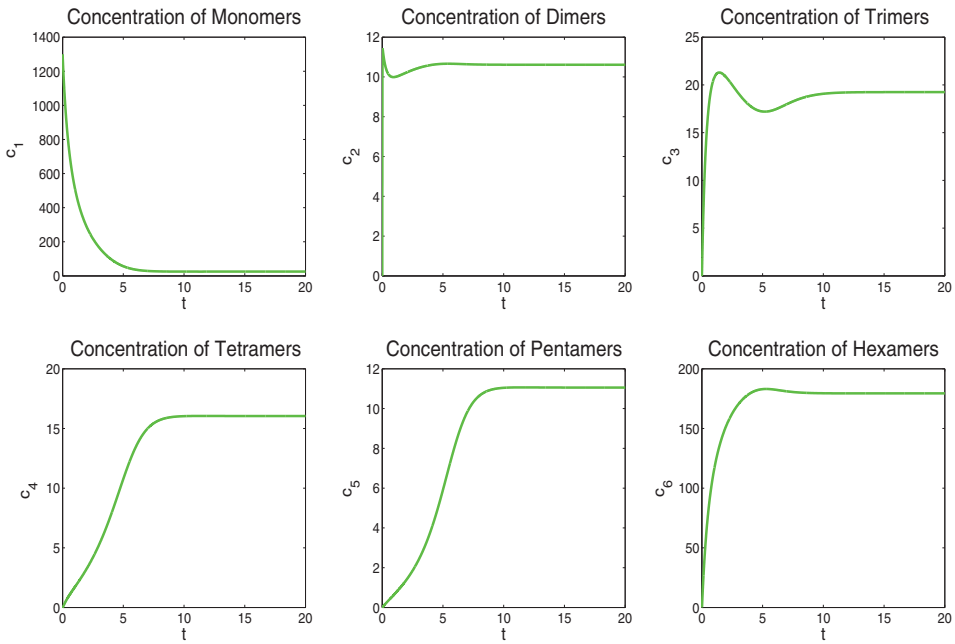

Fig. 7. Simulation results for the full model in Eq. (1): Concentrations of all intermediates $c_n (1 \le n \le 6)$ from simulation time $t = 0$ to $t = 20$ (s) with an initial condition $\vec{c}(0) = (c_1(0), c_2(0), c_3(0), c_4(0), c_5(0), c_6(0)) = (1300, 0, 0, 0, 0, 0)$. Simulations were performed until $t = 24 \times 3600$ (s), though they are not shown here due to the early convergence of the solution. These results are very similar to those shown in Fig 4.

The aforementioned parameter fitting and model reduction methodology can also be applied directly to the full model proposed in Section 1.1.

The full model (Eq. (1)) has 20 parameters, whereas the reduced model (Eq. (2)) has 16 parameters. Parameter fitting was applied to the reduced model and the fitted values were listed in Table 1. Parameter fitting is now applied to the full model and the fitted values are listed in Table 5, along with the values from Table 1. It can be observed from Table 5 that for the 16 parameters retained in the reduced model, their numerical values in these two rounds of fitting are very close.

For the full model with the fitted values of these 20 parameters, we perform also numerical simulations and plot the multimer concentrations (c_1 through c_6) in Fig. 7. It can be observed from Figs. 4 and 7 that these concentration profiles are very similar for the full model and the reduced model.

Furthermore, we perform elasticity analysis for the 20 parameters in the full model, in the same way as we did for the reduced model. As shown in Fig. 8, the parameters f_{23}, f_{33}, b_{53} have clearly very small magnitude in elasticity. These three parameters are among the four parameters $f_{23}, f_{33}, b_{63}, b_{53}$, which are in the reduction (from the full model to the reduced model) investigated in Sections 1.1 and 1.2.

5. Discussion

This paper focuses on the nucleation stage of viral capsid assembly. It is different than the existing work [12,18,26] that consider mainly one pathway and add/delete one capsomer unit at a time. Our model considers more pathways for association and dissociation and provides more information about the assembly. It is now revealed by the model that CA dimers indeed play an important role in the nucleation stage, as reflected in two results: (i) the initial spike in the dimer concentrations in the numerical simulations; (ii) analysis showing that f_{22}, f_{24}, f_{222} are important parameters for HIV-1 capsid nucleation. These results conform with the findings in [4,8,15,40].

Parameters f_{11}, f_{12}, b_{64} exhibit elasticity in the monomer and hexamer concentrations c_1, c_6. These three association or dissociation rates correspond respectively to three reactions: (i) two monomers forming a dimer; (ii) a monomer and dimer together producing a trimer; (iii) a hexamer breaking apart into a tetramer and dimer. Examination of elasticity at different times helps determine which pathway is the most important. For instance, after the initial spike of the concentration of dimers, the concentrations of the intermediates become more sensitive to f_{222}. This is an indication of the importance of three dimers forming a hexamer. These results imply that the most important pathways for hexamer formation are single monomers joining together and triple binding dimers. These results demonstrate that our model has predictability to a certain level.

This paper applies also sensitivity and elasticity analysis for model reduction by identifying insignificant or less important model parameters. The reduced model is validated by agreement of biological experiment data and *in silicon* results. In general, an alternation or perturbation of a dynamical system will result in the fundamental issue of global stability and/or bi-stability [32]. New mathematical tools

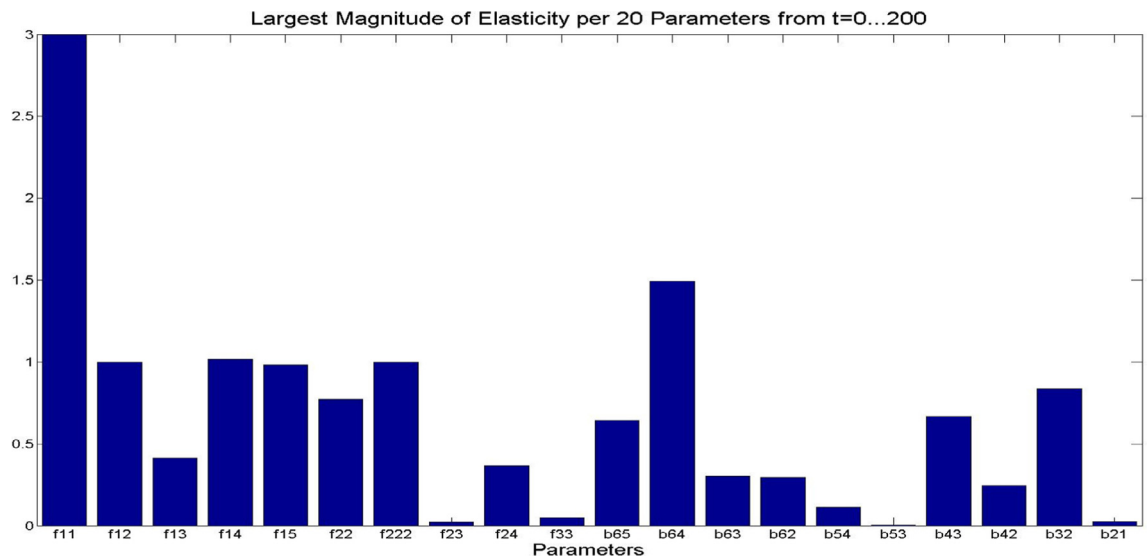

Fig. 8. The largest elasticity magnitudes for the 20 parameters of the full model (Eq. (1)).

like those in [39] need to be developed to address the global stability of the polynomial autonomous dynamical systems for viral capsid nucleation.

Clearly, there exists randomness in the nucleation stage of viral capsid assembly. The temperature, pH-value, and many other factors in the environment of assembly affect the association and dissociation rates and hence, the formation of CA hexameters and pentamers. Our future work includes investigation of the stochastic features of nucleation and stochastic dynamical systems will be an indispensable tool [2].

The investigation of nucleation cannot be completely isolated from the whole process of viral capsid assembly. It is our postulation that at the early stage of viral capsid assembly, hexamer formation happens simultaneously in many locations within the virion. Then these hexamers further assemble into the viral capsid. Pentamers might form at the places where it is difficult for a hexamer to form. This is the elongation stage. In other words, the products of nucleation serves as feed of the elongation stage. We foresee a cascade of kinetics and cascaded stochastic dynamical systems (CSDS) shall be an exploratory tool for this investigation.

Acknowledgments

Farrah Sadre-Marandi was partially supported by US National Science Foundation under grant IIA-141511 and Colorado State University Yates Graduate Fellowship. Yuewu Liu and Xiufen Zou were partially supported by the Major Research Plan of the National Natural Science Foundation of China (no. 91230118) and the National Natural Science Foundation of China (no. 61173060). Sadre-Marandi, Liu, and Tavener would like to express their sincere thanks to Prof. Chaoping Chen of Department of Biochemistry and Molecular Biology at Colorado State University for her great help and the stimulating discussion.

References

[1] A. Alfadhli, D. Huseby, E. Kapit, D. Colman, E. Barklis, Human immunodeficiency virus type 1 matrix protein assembles on membranes as a hexamer, J. Virol. 81 (2006) 1472–1478.
[2] J.E. Baschek, H. Klein, U.S. Schwarz, Stochastic dynamics of virus capsid formation: direct versus hierarchical self-assembly, BMC Biophys. 5 (2012) 1–18.
[3] J. Benjamin, B.K. Ganser-Pornillos, W.F. Tivol, W.I. Sundquist, G.J. Jensen, Three-dimensional structure of HIV-1 virus-like particles by electron cryotomography, J. Mol. Biol. 346 (2005) 577–588.
[4] L. Briant, B. Gay, C. Devaux, N. Chazal, HIV-1 assembly, release, and maturation, World J. AIDS 1 (2011) 111–130.
[5] J. Briggs, K. Grünewald, B. Glass, F. Förster, H.-G. Kräusslich, S.D. Fuller, The mechanism of HIV-1 core assembly: Insights from three-dimensional reconstructions of authentic virions, Structure 14 (2006) 15–20.
[6] J. Briggs, H.G. Kräusslich, The molecular architecture of HIV, J. Mol. Biol. 410 (2011) 491–500.
[7] J. Briggs, J.D. Riches, B. Galss, V. Bartonova, G. Zanetti, H.G. Kräusslich, Structure and assembly of immature HIV, PNAS 106 (2009) 11090–11095.
[8] I.L. Byeon, X. Meng, J. Jung, G. Zhao, R. Yang, J. Ahn, J. Shi, J. Concel, C. Aiken, P. Zhang, A.M. Gronenborn, Structural convergence between Cryo-EM and NMR reveals intersubunit interactions critical for HIV-1 capsid function, Cell 139 (2009) 780–790.
[9] D. Caspar, A. Klug, Physical principles in the construction of regular viruses, Cold Spring Harb. Symp. Quant. Biol. 27 (1962) 1–24.
[10] B. Chen, R. Tycko, Simulated self-assembly of the HIV-1 capsid: Protein shape and native contacts are sufficient for two-dimensional lattice formation, Biophys. J. 100 (2011) 3035–3044.
[11] R.C. Eberhart, J. Kennedy, A new optimizer using particle swarm theory, in: Proceedings of the Sixth International Symposium on Micro Machine & Human Science, 1, 1995, pp. 39–43.
[12] D. Endres, A. Zlotnick, Model-based analysis of assembly kinetics for virus capsids or other spherical polymers, Biophys. J. 83 (2002) 1217–1230.
[13] B. Ganser-Pornillos, A. Cheng, M. Yeager, Structure of full-length HIV-1 CA: a model for the mature capsid lattice, Cell 131 (2007) 70–79.
[14] B. Ganser-Pornillos, M. Yeager, O. Pornillos, Assembly and architecture of HIV, Viral Mol. Mach. 726 (2008) 441–465.
[15] B. Ganser-Pornillos, M. Yeager, W.I. Sundquist, The structural biology of HIV assembly, Struct. Biol. 18 (2008) 203–217.
[16] J. Grime, G.A. Voth, Early stages of the HIV-1 capsid protein lattice formation, Biophys. J. 103 (2012) 1774–1783.
[17] M. Hagan, Modeling viral capsid assembly, Adv. Chem. Phys. 155 (2014) 1–34.
[18] M. Hagan, O. Elrad, Understanding the concentration dependence of viral capsid assembly kinetics – the origin of the lag time and identifying the critical nucleus size, Biophys. J 98 (2010) 1065–1074.
[19] S. Jin, L. Niu, G. Wang, X. Zou, Mathematical modeling and nonlinear dynamical analysis of cell growth in response to antibiotics, Int. J. Bifurc. Chaos 25 (2015). Article ID: 1540007, 12 pages, doi:10.1142/S0218127415400076.
[20] S. Katen, A. Zlotnick, The thermodynamics of virus capsid assembly, Methods Enzymol. 455 (2009) 395–417.
[21] N. Komarova, D. Levy, D. Wodarz, Effect of synaptic transmission on viral fitness in HIV infection, PLoS ONE 7 (2012) E48361.
[22] J. Lanman, T.T. Lam, S. Barnes, M. Sakalian, M.R. Emmett, A.G. Marshall, P.E. Preveige, Identification of novel interactions in HIV-1 capsid protein assembly by high-resolution mass spectrometry, J. Mol. Biol. 325 (2003) 759–772.
[23] S. Li, C.P. Hill, W.I. Sundquist, J.T. Finch, Image reconstructions of helical assemblies of the HIV-1 CA protein, Nature 407 (2000) 409–413.
[24] S. Liu, L. Pang, S. Ruan, X. Zhang, Global dynamics of avian influenza epidemic models with psychological effect, Comput. Math. Methods Med. 2015. Article ID 913726, 12 pages.
[25] K. Mayo, D. Huseby, J. McDermott, B. Arvidson, L. Finlay, E. Barklis, Retrovirus capsid protein assembly arrangements, J. Mol. Biol. 325 (2003) 225–237.
[26] R. Munoz-Alicea, HIV-1 Gag Trafficking and Assembly: Mathematical Models and Numerical Simulations, Colorado State University, 2013 (Ph.D. dissertation.
[27] O. Pornillos, B.K. Ganser-Pornillos, M. Yeager, Atomic-level modelling of the HIV capsid, Nature 469 (2011) 424–428.

[28] O. Pornillos, B. Ganser-Pornillos, M. Yeager, Disulfide bond stabilization of the hexameric capsomer of human immunodeficiency virus, J. Mol. Biol. 401 (2010) 985–995.
[29] Protein Data Bank,http://www.rcsb.org/pdb/home/home.do.
[30] O. Pornillos, B. Ganser-Pornillos, B. Kelly, Y. Hua, F. Whitby, C. Stout, W. Sundquist, C. Hill, M. Yeager, X-ray structures of the hexameric building block of the HIV capsid, Cell 137 (2009) 1282–1292.
[31] L. Roeger, Z. Feng, C. Castillo-Chavez, Modeling TB and HIV co-infections, Math. Biosci. Eng. 6 (2009) 815–837.
[32] M. Shub, Global Stability of Dynamical Systems, Springer, 1987.
[33] J.K. Stille, Step-growth polymerization, J. Chem. Educ. 58 (1981) 862–866.
[34] W. Sundquist, H. Kräusslich, HIV-1 assembly, budding, and maturation, Cold Spring Harbor Perspect Med. 2 (2012) 1–24.
[35] J. Tan, X. Zou, Optimal control strategy for abnormal innate immune response, Comput. Math. Meth. Med. (2015) 386235, doi:10.1155/2015/386235.
[36] J. Tan, X. Zou, Complex dynamical analysis of a coupled system from innate immune responses, Int. J. Bifur. Chaos 23 (2013). Article ID: 1350180, 26 pages.
[37] S. Tavener, M. Mikucki, S. Field, M.F. Antolin, Transient sensitivity analysis for nonlinear population models, Methods Ecol. Evol. 2 (2011) 560–575.
[38] S. Tavener, M. Mikucki, Sensai: A matlab package for sensitivity analysis, http://www.math.colostate.edu/~tavener/FEScUE/SENSAI/sensai.shtml.
[39] J.P. Tian, J. Wang, Global stability for cholera epidemic models, Math. Biosci. 232 (2011) 31–41.
[40] B.G. Turner, M.F. Summers, Structural biology of HIV, J. Mol. Biol. 285 (1999) 1–32.
[41] Y. Wang, J. Tan, F. Sadre-Marandi, J. Liu, X. Zou, Mathematical modeling for intracellular transport and binding of HIV-1 gag proteins, Math. Biosci. 262 (2015) 198–205.
[42] D. Wodarz, Mathematical models of HIV replication and pathogenesis, Methods Mol. Biol. 1184 (2014) 563–581.
[43] M. Yeager, Design of in vitro symmetric complexes and analysis by hybrid methods reveal mechanisms of HIV capsid assembly, J. Mol. Biol. 410 (2011) 534–552.
[44] G. Zhao, J. Perilla, E. Yufenyuy, X. Meng, B. Chen, J. Ning, J. Ahn, A. Gronenborn, K. Schulten, C. Aiken, P. Zhang, Mature HIV-1 capsid structure by cryo-electron microscopy and all-atom molecular dynamics, Nature 497 (2013) 642–646.
[45] A. Zlotnick, J.M. Johnson, P.W. Wingfield, S.J. Stahl, D. Endres, A theoretical model successfully identifies features of hepatitis b virus capsid assembly, Biochem. 38 (1999) 14644–14652.